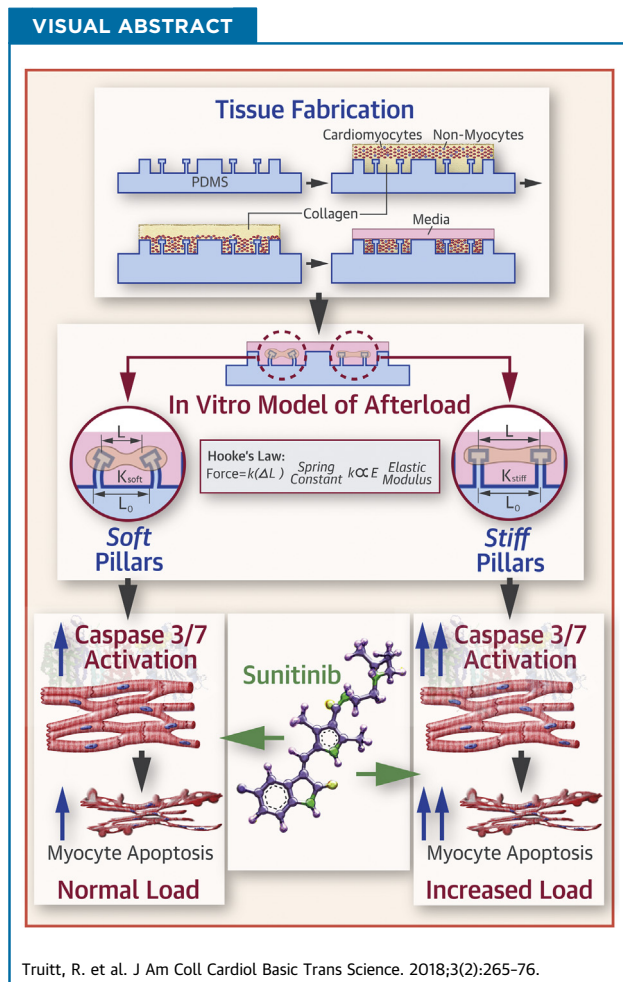


PRECLINICAL RESEARCH

Increased Afterload Augments Sunitinib-Induced Cardiotoxicity in an Engineered Cardiac Microtissue Model



Rachel Truitt, PhD,^{a,b} Anbin Mu,^b Elise A. Corbin, PhD,^{b,c} Alexia Vite, PhD,^b Jeffrey Brandimarto, PhD,^b Bonnie Ky, MD, MSCE,^{b,d} Kenneth B. Margulies, MD^b



HIGHLIGHTS

- Sunitinib, an oral tyrosine kinase inhibitor used widely to treat solid organ tumors, frequently induces hypertension and causes LV dysfunction in up to 19% of treated individuals.
- Sunitinib-induced cardiotoxicity can be modeled using engineered CMT.
- In CMT, sunitinib induces dose- and duration-dependent activation of apoptosis pathways and decreases in CMT force generation, spontaneous beating, and mitochondrial membrane potential.
- Exposure of CMT to increased in vitro afterload intensifies the cardiotoxicity of clinically relevant sunitinib concentrations.
- These findings suggest that intensive antihypertensive therapy may be an appropriate strategy to mitigate LV dysfunction observed in patients treated with sunitinib.

From the ^aDepartment of Bioengineering, School of Engineering and Applied Sciences, University of Pennsylvania, Philadelphia, Pennsylvania; ^bCardiovascular Institute, Perelman School of Medicine, University of Pennsylvania, Philadelphia, Pennsylvania; ^cDepartment of Mechanical Engineering and Applied Mechanics, School of Engineering and Applied Sciences, University of Pennsylvania, Philadelphia, Pennsylvania; and the ^dCenter for Clinical Epidemiology and Biostatistics, Perelman School of Medicine, University of Pennsylvania, Philadelphia, Pennsylvania. Supported by the National Center for Research Resources, grant

ABBREVIATIONS AND ACRONYMS

2D = 2-dimensional

3D = 3-dimensional

AICAR = 5-aminoimidazole-4-carboxamide 1- β -D-ribofuranoside

AMPK = adenosine monophosphate-activated protein kinase

ATP = adenosine triphosphate

CCCP = carbonyl cyanide *m*-chlorophenyl hydrazine

CMT = cardiac microtissue

DMSO = dimethyl sulfoxide

EDTA = ethylenediamine tetraacetic acid

huMSC = human mesenchymal stem cell

Hu-IPS-CM = human induced pluripotent stem cell cardiomyocyte

IPS-CM = induced pluripotent stem cell-derived cardiomyocyte

LV = left ventricle

NRVM = neonatal rat ventricular myocyte

PDMS = polydimethylsiloxane

RPMI = Roswell Park Memorial Institute medium

TMRM = tetramethylrhodamine

SUMMARY

Sunitinib, a multitargeted oral tyrosine kinase inhibitor, used widely to treat solid tumors, results in hypertension in up to 47% and left ventricular dysfunction in up to 19% of treated individuals. The relative contribution of afterload toward inducing cardiac dysfunction with sunitinib treatment remains unknown. We created a preclinical model of sunitinib cardiotoxicity using engineered microtissues that exhibited cardiomyocyte death, decreases in force generation, and spontaneous beating at clinically relevant doses. Simulated increases in afterload augmented sunitinib cardiotoxicity in both rat and human microtissues, which suggest that antihypertensive therapy may be a strategy to prevent left ventricular dysfunction in patients treated with sunitinib. (J Am Coll Cardiol Basic Trans Science 2018;3:265-76) © 2018 The Authors. Published by Elsevier on behalf of the American College of Cardiology Foundation. This is an open access article under the CC BY-NC-ND license (<http://creativecommons.org/licenses/by-nc-nd/4.0/>).

The rise of small molecule inhibitors targeting receptor tyrosine kinases that regulate tumor vasculature angiogenesis and cellular proliferation have resulted in important gains in cancer survival (1). However, many of these “targeted” therapies have unintended consequences on the cardiovascular system (2-5). Sunitinib, a multitargeted tyrosine kinase inhibitor used widely in the treatment of renal cell carcinoma, gastrointestinal stromal tumors, and neuroendocrine tumors, is currently under investigation in over 500 active clinical trials (6-8). However, among sunitinib-treated patients, hypertension occurs in 11% to 43% of patients and left ventricular (LV) dysfunction

in up to 19% (9-11). These toxicities, although often manageable, can result in dose reduction or treatment interruption, which can affect oncologic outcomes.

SEE PAGE 277

Cardiovascular toxicity with sunitinib has been hypothesized to be a result of off-target inhibition of receptor tyrosine kinases and mitochondrial function that are important for maintaining cardiovascular homeostasis (3,6,12-14), particularly during states of increased stress (15-19). However, the relative contribution of each of these factors remains poorly understood. Another contributing factor that may be critical in the development of LV dysfunction during

sunitinib treatment is hypertension (20-22). More specifically, it is not clear whether hypertension unmasks LV dysfunction or actually lowers the threshold for sunitinib cardiotoxicity. We hypothesized that increased afterload augments the cardiotoxic effects of sunitinib.

Testing this hypothesis in humans would likely require substantial resources and involve ethical challenges with cohorts of patients with untreated hypertension. Current in vitro cell culture and animal models also suffer from limitations that minimize their usefulness for modeling how biomechanical influences affect sunitinib cardiotoxicity in humans (23,24). Thus, we used an engineered in vitro 3-dimensional (3D) cardiac microtissue (CMT) model incorporating cardiomyocytes from neonatal rats or human pluripotent stem cells that self-assemble onto polydimethylsiloxane (PDMS) pillars (25,26). We used this system to characterize sunitinib cardiotoxicity using metrics for cell viability, mitochondrial dysfunction, and cardiac function, and examined how these characteristics are affected by sunitinib dose, treatment duration, and the magnitude of biomechanical loading.

METHODS

CMT PLATFORM. CMT arrays were fabricated as previously described (25,26) (Supplemental Appendix). Devices were cast from PDMS pre-polymer (5:1 to 15:1

UL1RR024134; the National Center for Advancing Translational Sciences, grant UL1TR000003; and in part by the University of Pennsylvania's Institute for Translational Medicine and Therapeutics (ITMAT) Transdisciplinary Program in Translational Medicine and Therapeutics. Dr. Truitt received support from the American Heart Association Predoctoral Fellowship (11PRE7610168) and National Science Foundation Graduate Research Fellowship (2011125128) programs. Dr. Ky has received Pfizer's Investigator Initiated Award. All other authors have reported that they have no relationships relevant to the contents of this paper to disclose. All authors attest they are in compliance with human studies committees and animal welfare regulations of the authors' institutions and Food and Drug Administration guidelines, including patient consent where appropriate. For more information, visit the *JACC: Basic to Translational Science* [author instructions page](#).

base to curing agent ratio) to create devices with stiff and soft pillars, respectively. Unless otherwise stated, arrays used in this study were created using a 5:1 base to curing ratio of PDMS.

MICROTISSUE SEEDING PROCEDURE. Microtissues derived from neonatal rat ventricular myocytes (NRVM) were prepared, as previously described (26) (Supplemental Appendix). CMTs, derived from human-induced pluripotent stem cell cardiomyocytes (Hu-iPS-CM) were prepared in the same manner as rat CMT with a few exceptions. Specifically, monolayers of beating Hu-iPS-CM (days 16 to 30) were detached from culture plates using TrypLE Express (Gibco, Thermo Fisher Scientific, Waltham, Massachusetts) for 7 to 10 min at 37°C with 5% CO₂. Human mesenchymal stem cells (huMSC) were detached from culture plates with 0.05% Trypsin ethylenediamine tetraacetic acid (EDTA) for 5 min at 37°C with 5% CO₂. Hu-iPS-CM and huMSC were mixed to create tissues composed of 93% CM per 7% huMSC. Tissues were maintained in Roswell Park Memorial Institute medium (RPMI) + 20% fetal bovine serum + 100 U/ml penicillin/streptomycin + 5 μmol/l Y27632 media for the first 24 h and then switched to RPMI + B27 (plus insulin) + 1% penicillin/streptomycin media, which was exchanged every 2 days. Experiments were performed on day 5 of microtissue culture.

DRUG STUDIES. Stock solutions (10 mmol/l) of Sunitinib malate (S-8803, LC Laboratories, Woburn, Massachusetts) were prepared in dimethyl sulfoxide (DMSO) (D12345, Life Technologies, Thermo Fisher Scientific) and were remade every 6 months to ensure biological activity. Stock solutions were diluted at least 1:1000 in media for experiments to avoid any DMSO-induced toxicity. Samples treated with DMSO at the same volume per volume percentage were used as control samples (vehicle). Microtissues treated with 1 μmol/l Staurosporine (Sigma Aldrich, St. Louis, Missouri) were used as a positive control for apoptosis (27). Carbonyl cyanide *m*-chlorophenyl hydrazone (CCCP) (Sigma Aldrich) was used a positive control for mitochondria membrane potential disruption (28) at a concentration of 50 μmol/l and was incubated with cells for 30 min at 37°C. In a subset of experiments, 5-aminoimidazole-4-carboxamide 1-β-D-ribofuranoside (AICAR) (Sigma Aldrich) was administered concurrently with sunitinib at a concentration of 1 mmol/l.

CASPASE 3/7 ACTIVATION. Activated caspase 3/7 levels were measured using the Caspase-Glo 3/7 assay (Promega Corporation, Madison, Wisconsin), according to the manufacturer's instructions.

Microtissue arrays were washed with Dulbecco phosphate-buffered saline (without Ca²⁺, Mg²⁺) to remove residual media. At least 6 to 12 tissues were collected per experimental sample. Samples were pipetted and vortexed to completely lyse tissues and analyzed on BioTek Synergy H1 Multi-Mode plate reader (Winooski, Vermont) equipped with Gen5.0 software.

CELL VIABILITY ASSAY. Cell viability was assessed by trypan blue exclusion (29). Briefly, whole microtissue arrays were digested in a 1 mg/ml collagenase IV (Gibco) solution in Dulbecco phosphate-buffered saline (with Ca⁺⁺, Mg⁺⁺) with 10% fetal bovine serum for 15 min at 37°C to digest collagen I gel. Tissues were further broken down into single cells by dissociating with 0.05% Trypsin EDTA.

MICROTISSUE FORCE GENERATION MEASUREMENTS. Static (diastolic) tension was inferred by measuring the displacement of pillars, as previously described (26). Images were acquired using a 10× Plan Fluor objective on a Nikon TE2000U inverted microscope equipped with QImaging Exi Blue camera (Surry, British Columbia, Canada) and NIS-Elements BR software (Nikon Instruments, Melville, New York). Images were taken from the bottom, middle, and top of the microwells. The width of a single cap (ϕ), as well as the separation between caps (S) and bases of pillars (B) was measured in ImageJ (National Institutes of Health, Bethesda, Maryland) in units of pixels. We derived the displacement (μm) of the pillar using the formula provided in Equation 1, where 0.1706 is the conversion factor between pixels and microns for the objective used in these experiments.

$$\text{Displacement } \delta (\mu\text{m}) = \frac{B - (S + \phi)}{0.1706 \frac{\text{pixels}}{\mu\text{m}}} \quad (1)$$

For active (systolic) tension measurements, fluorescence videos were captured and displacements of fluorescent beads imbedded into caps of pillars were traced in ImageJ as previously described (26).

MITOCHONDRIAL MEMBRANE POTENTIAL MEASUREMENTS. NRVM were cultured in 24-well plates for 24 to 48 h post-isolation before any drug treatments. Cells were treated with 1 μmol/l sunitinib for 30 min to 24 h. Cells were labeled with 10 nmol/l tetramethylrhodamine (TMRM), methyl ester perchlorate (Life Technologies, Thermo Fisher Scientific) in serum-free media, as previously described (30). Samples were analyzed on a Beckman Dickinson LSRII Flow Cytometer equipped with a 488-nm blue laser for excitation and 575/26 emission filter to measure TMRM. Post-experimental analysis of data was performed using Flow Jo V10 software (FlowJo

LLC, Ashland, Oregon). The TMRM high population within the TMRM positive plot was quantified using the 575/26 histogram plot, where a shift to the left indicates lower levels of TMRM fluorescence and therefore decreased mitochondrial membrane potential.

ATP ASSAY. Adenosine triphosphate (ATP) levels were quantified using the ATP assay from Calbiochem (EMD Millipore, Burlington, Massachusetts) according to the manufacturer's instructions. Using NRVM cultured in a conventional 2-dimensional (2D) format, plates were analyzed on a BioTek Synergy H1 Multi-Mode plate reader equipped with Gen5.0 software. To ensure that total protein content did not significantly vary between experimental samples, protein readings were performed using a Qubit system (Thermo Fisher Scientific) according to the manufacturer's instructions.

STATISTICAL ANALYSIS. All graphs were plotted as mean \pm SD; except for box-and-whisker plots where error bars extend from median to minimum and maximum values. Individual experiments measuring caspase 3/7 and ATP levels were conducted with 3 technical replicates per experimental sample. In experiments utilizing trypan blue exclusion, at least 100 cells were counted per measurement and both chambers of hemocytometer were assayed to give 2 technical replicates per experimental group. Measurements of microtissue function, such as force generation and electrical parameters, were assayed on individual tissues. We tracked the functional changes in individual tissues instead of performing a bulk average before and after treatment, and thus results will be presented as the percentage of change from baseline measurements conducted before treatment. For experiments using flow cytometry, at least 20,000 cells were analyzed per experimental sample, and the percentage of TMRM high cells was calculated from this population. Unpaired 2-tail Student *t* tests were performed when appropriate (GraphPad QuickCalcs, GraphPad Software Inc., San Diego, California). To model the dose dependence of sunitinib-induced caspase 3/7 activation, caspase data was fit to a \log_2 function ($y = a \log_2 x + b$) using nonlinear regression in Microsoft Excel Solver (Redmond, Washington).

RESULTS

RAT CMT DEMONSTRATE DECREASES IN CELL VIABILITY FOLLOWING SUNITINIB TREATMENT. In CMT derived from NRVM, we first examined time- and dose-dependent effects of in vitro sunitinib exposure on apoptosis as indicated by caspase 3/7

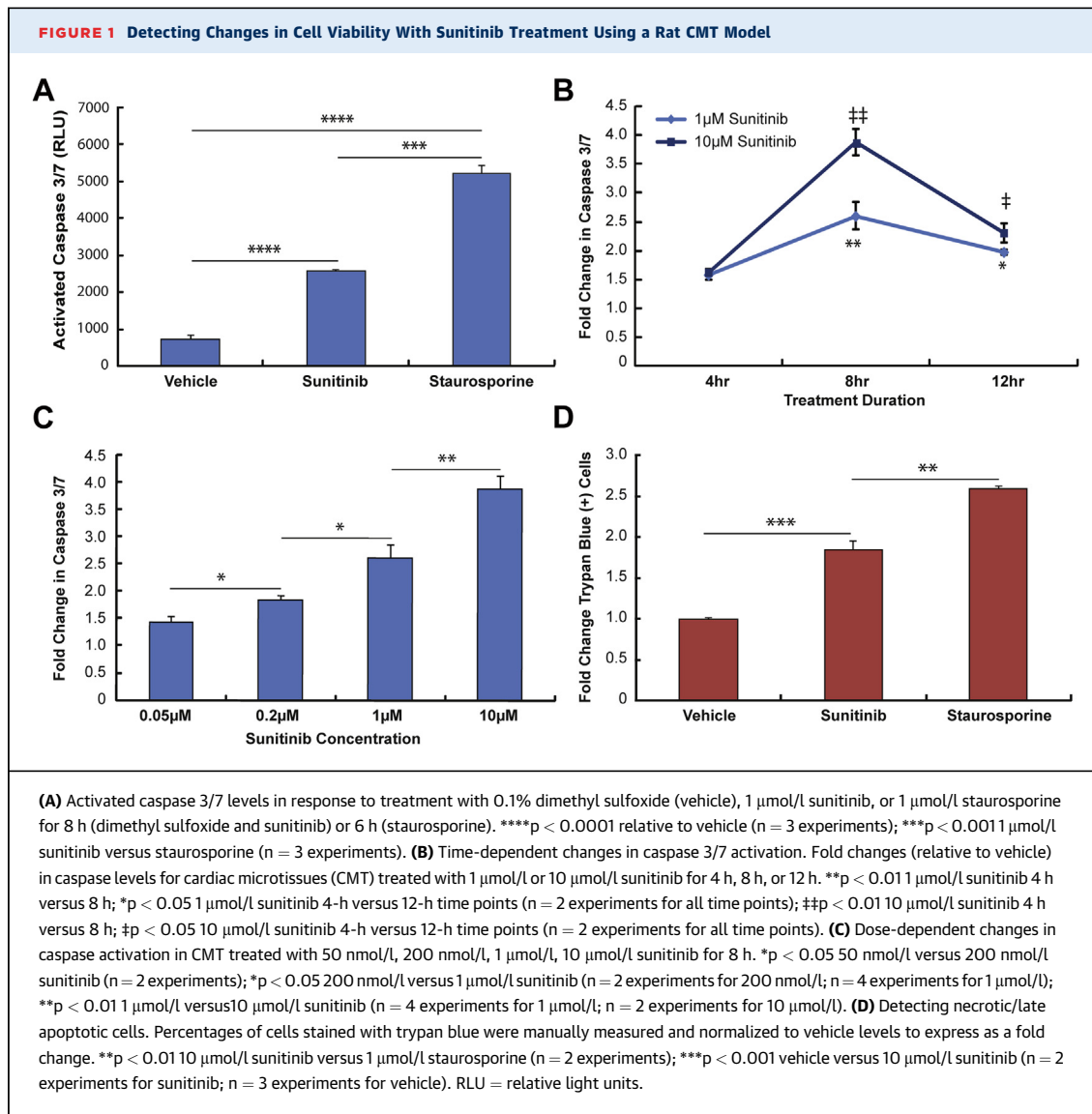
activation. We found that a clinically relevant concentration of sunitinib (1 $\mu\text{mol/l}$) induced significant activation of caspases 3 and 7, though to a lesser degree than the positive control staurosporine did (Figure 1A). Also, we found that caspase activation reached a maximum level at 8 h in CMT treated with 1 $\mu\text{mol/l}$ and 10 $\mu\text{mol/l}$ sunitinib (Figure 1B). All subsequent experiments examined caspase 3/7 activation at 8 h regardless of dose.

We determined that 50 nmol/l was the threshold concentration for caspase activation for our model and observed dose-dependent increases in caspase 3/7 activation in the range of 50 nmol/l to 10 $\mu\text{mol/l}$ sunitinib (Figure 1C). Doses >10 $\mu\text{mol/l}$ were not deemed physiologically relevant to humans given that the clinically observed concentrations of sunitinib in human blood are typically 0.1 to 1.9 $\mu\text{mol/l}$. We found that the degree of caspase activation correlated strongly with sunitinib dose (Figure 1C). Using nonlinear curve fitting methods, our results fit strongly with a logarithmic (\log_2) function that produced an R^2 value >0.99 (Supplemental Figure 1). Finally, we found increased numbers of late apoptotic/necrotic cells in CMT treated with 10 $\mu\text{mol/l}$ sunitinib as compared to vehicle (DMSO)-treated cells after performing a trypan blue exclusion (Figure 1D).

Collectively, these results demonstrate the ability of the rat microtissue model to detect decreases in viability due to sunitinib treatment that is dependent on sunitinib dose and treatment duration. These results also established the dose and treatment duration for subsequent experiments.

RAT CMT REVEAL CHANGES IN CARDIAC FUNCTION FOLLOWING SUNITINIB TREATMENT.

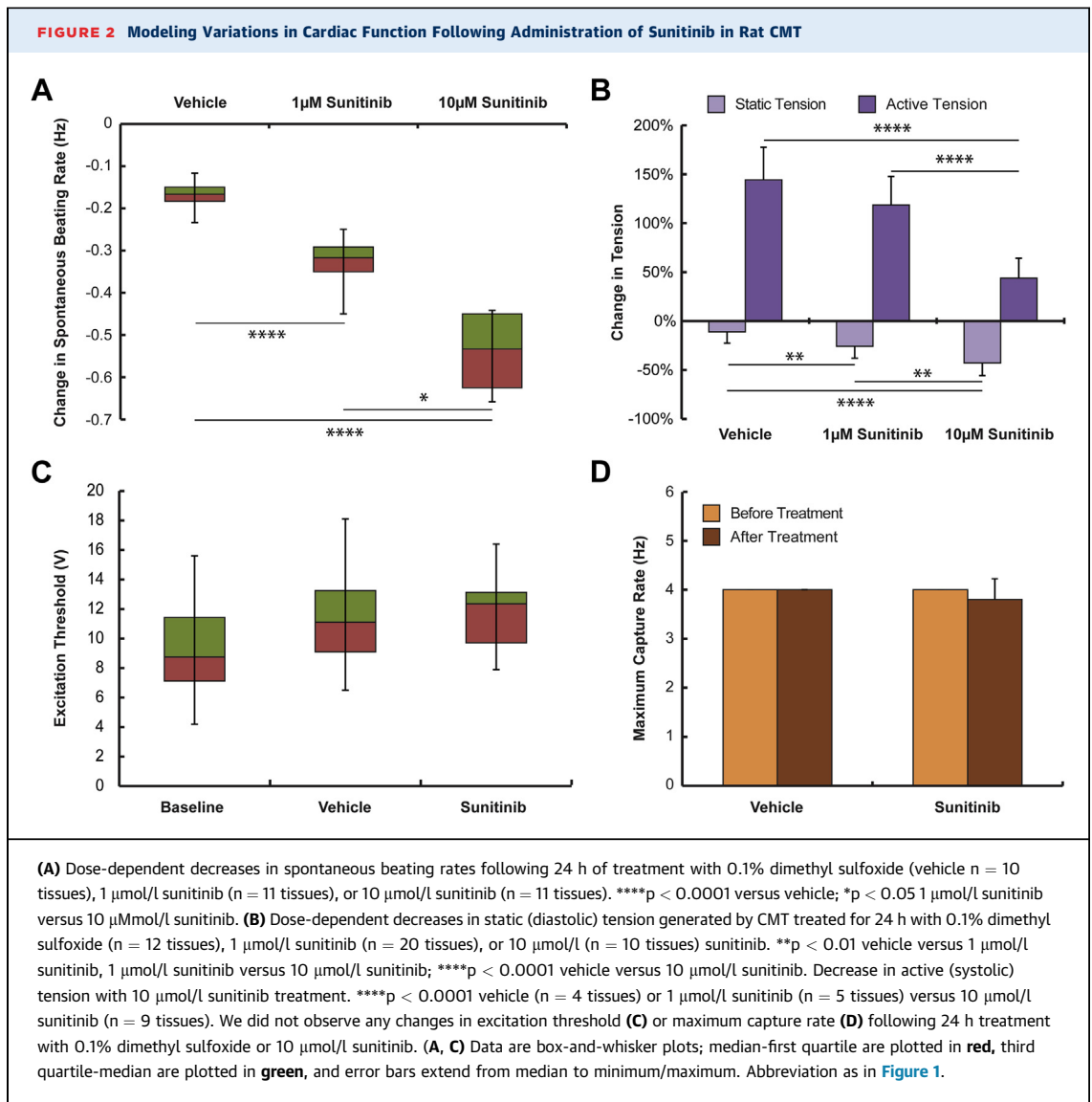
Cardiomyocyte dysfunction remains an important toxicity of sunitinib treatment; however, there are a limited number of studies characterizing changes in myocyte force generation and electrophysiological properties. We found that 1 $\mu\text{mol/l}$ sunitinib was sufficient to decrease the spontaneous beating rates of microtissues, and beating rates continued to decline in a dose-dependent manner (Figure 2A), with complete arrest at 10 $\mu\text{mol/l}$ sunitinib. Static (diastolic) forces generated by microtissues also decreased in a dose-dependent manner (Figure 2B). We found that active (systolic) force generation increased during the 24-h period of observation in vehicle-treated tissues, with tissues treated with 10 $\mu\text{mol/l}$ sunitinib showing significantly smaller increases in force generation (Figure 2B). When microtissues were subjected to field stimulation, we found neither significant differences in excitation threshold nor maximum capture rate between vehicle- and sunitinib-treated



tissues (Figures 2C and 2D). These results suggest that the rat CMT model serves as a robust tool for early detection of drug-induced cardiotoxicity, because it can detect parallel changes in cell viability and cardiac function.

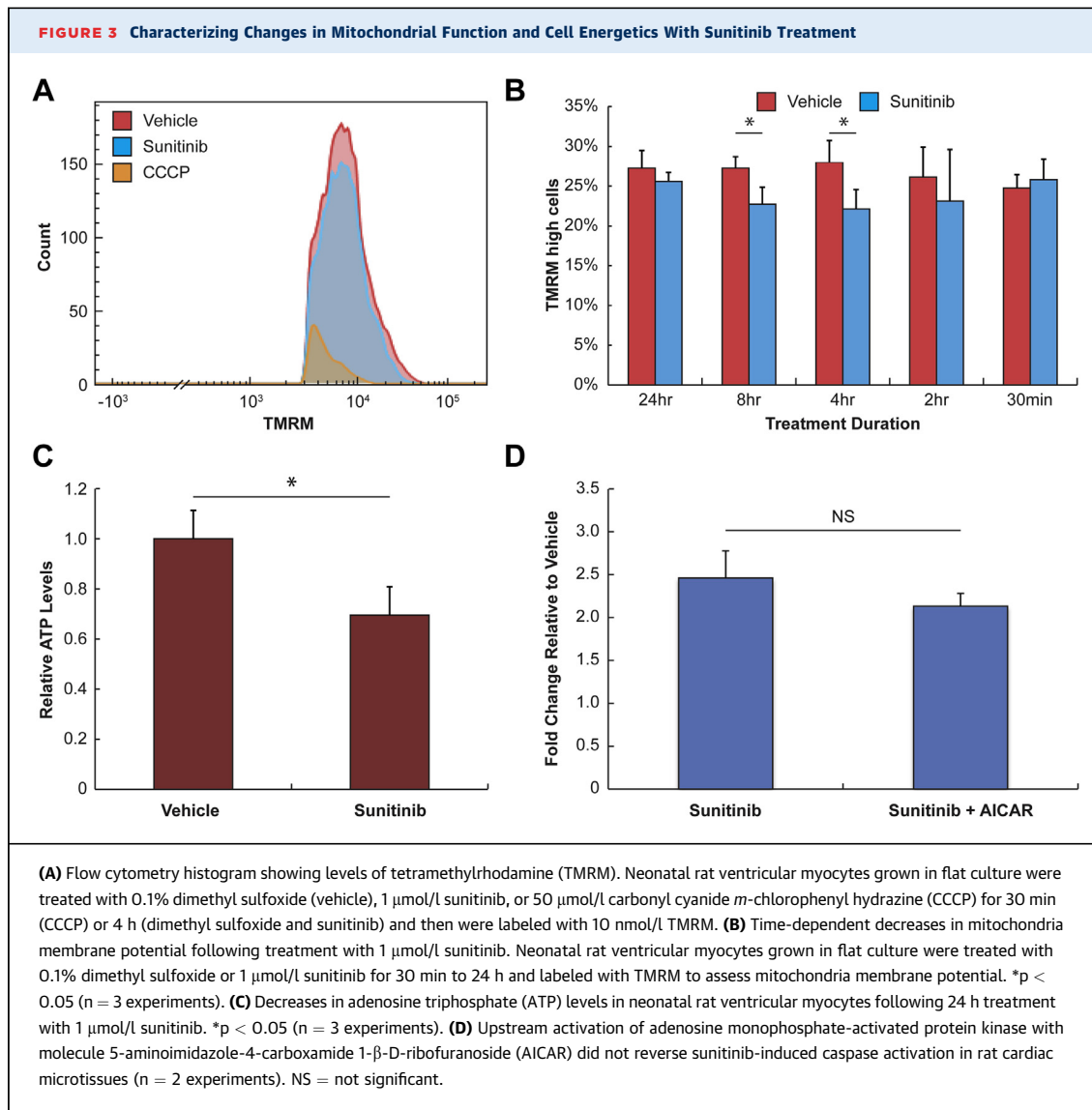
SUNITINIB INDUCES DECREASES IN MITOCHONDRIAL MEMBRANE POTENTIAL AND CELLULAR ATP LEVELS IN RAT CMT. Recognizing that mitochondrial dysfunction is a proposed mechanism of sunitinib cardiotoxicity, we assayed mitochondrial membrane potential in NRVM at various time points following treatment with 1 µmol/l sunitinib using TMRM and a flow cytometric analysis. We used CCCP, a known disruptor of mitochondrial membrane potential, as a positive control

for these experiments. Figure 3A shows a typical histogram of TMRM levels in vehicle-treated, sunitinib-treated (1 µmol/l), and CCCP-treated (50 µmol/l) NRVM. The plot demonstrates significant decreases in mitochondrial membrane potential with 1 µmol/l sunitinib treatment, although this change is relatively modest compared with the change seen with CCCP-treated cells. We hypothesized that like caspase activation, mitochondrial membrane potential may also exhibit time-dependent changes; therefore, we quantified differences in mitochondrial membrane potential between vehicle- and sunitinib-treated cells across various time points (Figure 3B). We found significant decreases in mitochondria membrane potential at 4-h and 8-h treatment durations, but none



before or after this time interval. Interestingly, these time points corresponded to peak caspase 3/7 activation. We also observed modest decreases in cellular ATP levels in NRVM treated with 1 $\mu\text{mol/l}$ sunitinib (Figure 3C). Previous studies have identified the inhibition of adenosine monophosphate-activated protein kinase (AMPK) activity as an off-target effect of sunitinib. We hypothesized that treating CMT with an AMPK activator, AICAR, could reverse caspase 3/7 activation. However, upstream activation of AMPK with AICAR was insufficient to attenuate caspase 3/7 activation in sunitinib-treated cells (Figure 3D). Our results reveal time-dependent changes in mitochondrial membrane potential with sunitinib treatment, which may contribute to observed decreases in cellular ATP levels.

CARDIOTOXIC EFFECTS OF SUNITINIB ARE AUGMENTED BY INCREASED IN VITRO AFTERLOAD IN THE RAT CMT MODEL. Recognizing that the pillar stiffness is the primary load constraining active shortening of the CMT, we cultured CMT for 48 h on stiff (5:1 base-to-curing ratio) and soft (15:1 base-to-curing ratio) pillars and treated them with either 0.1% DMSO (vehicle) or 1 $\mu\text{mol/l}$ sunitinib. Figure 4A shows caspase 3/7 activation for this experiment; in vehicle-treated CMT, we see greater caspase activation in soft pillars versus stiff pillars. However, in sunitinib-treated tissues, we observed greater caspase activation in stiff versus soft pillars, and that increased afterload augments sunitinib-induced caspase 3/7 activation (Figure 4B). These results suggest that increased in vitro afterload augments the

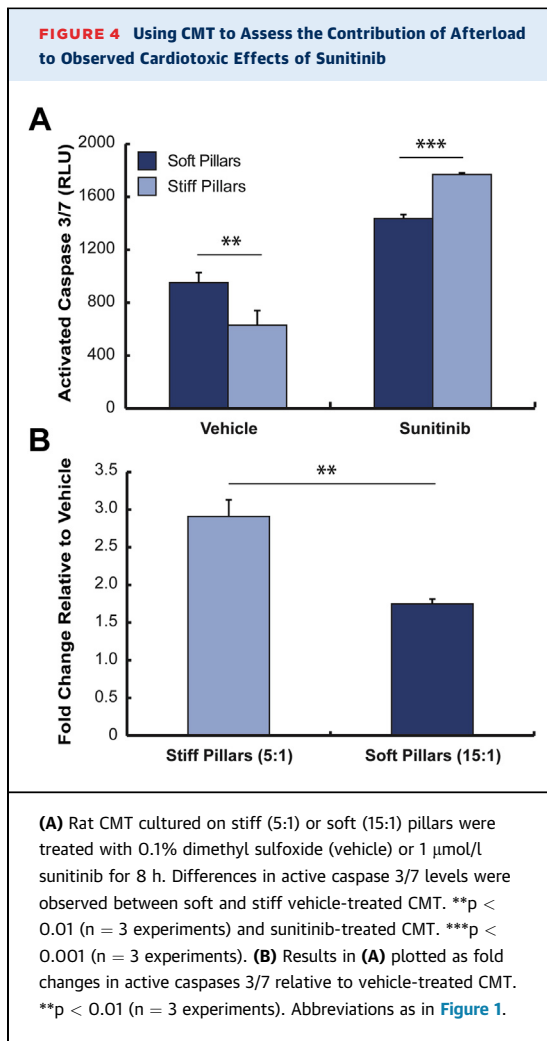


myocardial toxicity associated with a given dose and duration of sunitinib.

HUMAN CMT EXHIBIT AFTERLOAD-DEPENDENT CASPASE 3/7 ACTIVATION FOLLOWING SUNITINIB TREATMENT. We examined the responses of CMT composed of Hu-iPS-CM to sunitinib. Human CMT treated with 10 $\mu\text{mol/l}$ sunitinib for 8 h exhibited significant elevations in caspase 3/7 levels (Figure 5A). When we compared these responses to ones we obtained with rat CMT treated at the same concentration of sunitinib, we found that human CMT have nearly 3-fold greater caspase activation than rat CMT despite the absence of the established antiangiogenic sunitinib targets platelet-derived growth factor receptor-2 and vascular endothelial growth factor

receptor-2 (Supplemental Figure 2). When human CMT are treated with a more physiologically relevant dose of sunitinib (1 $\mu\text{mol/l}$), we found that caspase activation is very similar to what we observed in rat CMT (Figure 5A). These results suggest that human CMT exhibit robust toxicity responses to sunitinib.

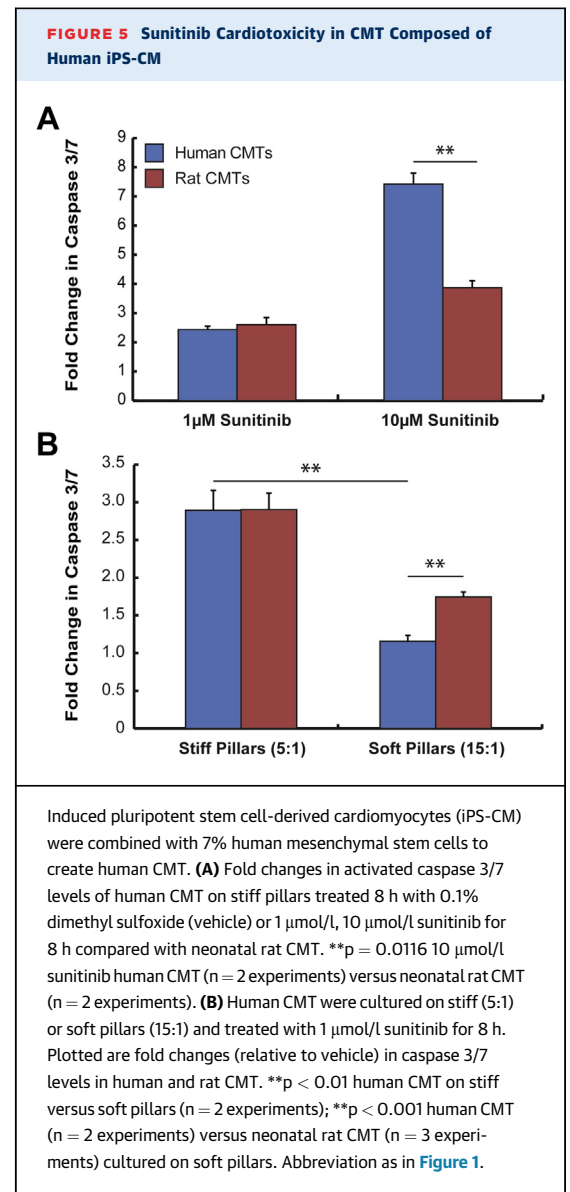
Next, we sought to address our hypothesis that increased in vitro afterload augments sunitinib cardiotoxicity in human CMT. Human CMT were cultured on both stiff and soft pillars for 5 days before being treated with 1 $\mu\text{mol/l}$ sunitinib. Using caspase 3/7 activation as a metric for cardiotoxicity, we found that human CMT cultured on stiff pillars exhibited increased caspase 3/7 activation following sunitinib treatment (2.43 ± 0.11 -fold vs. vehicle) compared with human CMT cultured on soft pillars (Figure 5B), which



demonstrated minimal increases in caspase 3/7 levels (1.15 ± 0.08 -fold vs. vehicle). Transcriptional profiling of fetal/hypertrophic genes prior to sunitinib exposure did not reveal significant expression differences based on pillar stiffness ([Supplemental Table 1](#), [Supplemental Figure 3](#)). These findings suggest that increased in vitro afterload potentiates the toxicity of sunitinib without significantly altering the baseline myocyte phenotype. In summary, increased in vitro afterload augments sunitinib-induced caspase 3/7 activation in human CMT.

DISCUSSION

Currently, more than 100,000 people have been treated with sunitinib, and there are over 500 open clinical trials with this drug listed at ClinicalTrials.gov; this fact stresses the need to improve our understanding of sunitinib-induced cardiotoxicity. Many basic and translational studies in cardio-oncology are



constrained by inadequate preclinical models. Animal models do not allow for precise control over biomechanical and biochemical factors (31). Likewise, the use of 2D cell cultures also suffers from serious shortcomings, such as inability to apply mechanical pre-load and afterload, which are essential features of cardiac physiology (32). Taking advantage of recent advances in tissue engineering, we created 3D CMT that better mimic in vivo conditions without sacrificing control over cellular, biochemical, and mechanical inputs. Using the CMT platform, we successfully created a preclinical cardiomyocyte model for characterizing sunitinib toxicity and used this model to gain insights into the mechanisms of sunitinib toxicity. These studies establish a template

for broader preclinical analysis of cardiomyocyte toxicity for the thousands of tyrosine kinase inhibitors currently in development.

First, we confirmed our CMT model could recapitulate previously observed increases in cell death with sunitinib treatment. We detected significant increases in caspase 3/7 activation following treatment of physiological doses of sunitinib, which is consistent with reports by others (33,34). To our knowledge, we are the first to report that the degree of caspase 3/7 activation correlates logarithmically (\log_2) with sunitinib dose. Additionally, we confirmed that caspase activation was time-dependent, a finding that has also been reported by others (33). Our results also demonstrated that many of these early apoptotic cells go on to become nonviable, providing a basis for elevated troponin levels in patients (35), creatine kinase-myocardial band elevations in rodent studies (36), and increases in terminal deoxynucleotidyl transferase 2'-deoxyuridine 5'-triphosphate nick end labeling-positive cells in in vitro NRVM studies (35).

Our microtissue model detected dose-dependent decreases in spontaneous beating rate and cessation of spontaneous contraction at 10 $\mu\text{mol/l}$ sunitinib. We postulate that these dose-dependent decreases in beating may be connected to inhibition of human ether-à-go-go-related gene channels because this has been shown to result in arrhythmias in neonatal rodent cells (37,38). We also observed dose-dependent decreases in static (diastolic) and active (systolic) tension generated by microtissues. These findings differ slightly from those of Rainer et al. (39) who reported decreases in systolic but not diastolic stresses in short-term (30 min) sunitinib experiments (doses ≥ 1.87 $\mu\text{mol/l}$) performed on human atrial muscle strips. These differences may be explained by the fact that reduced diastolic tension likely increased diastolic length, which could conceal decreases in systolic tension due to sunitinib, particularly in experiments where we treated with low doses of sunitinib (1 $\mu\text{mol/l}$).

In addition to creating a preclinical model for sunitinib cardiotoxicity, our studies provide insights about the mechanisms of this toxicity. First, our findings of toxicity in a CMT model that is not dependent on an intact circulation support the potential for direct toxicity of sunitinib, independent of vascular effects. These findings are consistent with the findings of Kerkela et al. (14) who implicated sunitinib-induced inhibition of cyclic AMPK as a mechanism for in vitro and in vivo cardiotoxicity with sunitinib. In this regard, the 1 $\mu\text{mol/l}$ dose found to be consistently toxic in our studies was above the half maximal effective concentration for AMPK (0.216 $\mu\text{mol/l}$), as defined by

Kerkela et al. (14). In addition, findings of modest, yet significant, decreases in mitochondrial membrane potential with sunitinib treatment complements patient biopsies showing swollen mitochondria and in vitro studies showing qualitative decreases in mitochondrial membrane potential at a single time point (14,35,40). Though sunitinib-induced caspase activation and changes in mitochondrial membrane potential appeared to peak at 8 h after exposure, reductions in spontaneous beating rate and force generation were most apparent at 24 h after initiation of sunitinib. This sequence suggests reductions in contractility are likely secondary to the metabolic disturbances and resulting cytotoxicity rather than a direct negative inotropic effect of sunitinib. It has been previously shown that activation of caspases 3 and 7 are key mediators of mitochondrial apoptosis events, such as decreases in membrane potential (40-42). Therefore, sunitinib may be directly affecting mitochondrial function or indirectly via caspase 3/7 activation. We further observed modest decreases in ATP levels, and these may be consequent to the changes in mitochondrial membrane integrity. Our findings of direct sunitinib-induced toxicity in vitro, do not preclude additional contributions of microvascular abnormalities in vivo. This might include defects in coronary flow reserve associated with pericyte loss, as implicated by Chintalgattu et al. (43) or attenuated increases in coronary capillary density during pressure overload, as implicated by Izumiya et al. (15). From this perspective, differences in rates of cardiotoxicity observed with alternative vascular endothelial growth factor-signaling pathway inhibitors might reflect differences in their potential for direct myocardial toxicity that could exacerbate the impact of in vivo microvascular effects.

The CMT model is particularly well suited for providing insight into whether increases in afterload augment cardiotoxic effects of sunitinib. We varied in vitro afterload by altering the stiffness of the pillars to which CMT are tethered and observed an increased magnitude of sunitinib-associated caspase activation with stiff pillars. When CMT are cultured on stiff pillars in the absence of sunitinib, we actually observed somewhat lower caspase activation, further supporting an interaction between sunitinib and increased in vitro afterload. Our results suggest that afterload is a key mediator of sunitinib's effects on LV function. We believe these results have direct clinical implications: early administration of antihypertensive therapy to patients on sunitinib may be useful in preventing subsequent LV dysfunction.

Finally, we examined responses of Hu-iPS-CM to sunitinib. We found the human CMT exhibited significant activation of caspase 3/7 in response to 10 $\mu\text{mol/l}$ sunitinib, more than 3 \times what we observed in rat CMT (Figure 5A). This difference is possibly species-related or maturation-related. Our results are in stark contrast to other studies using iPS-CM that required much higher concentrations of sunitinib to see decreases in cell viability (caspase activation and/or lactate dehydrogenase release) in 2D cultures (44). These differences may be due to differences in iPS-CM derivation and/or choice of culture platform (2D vs. 3D). However, our finding that increased in vitro afterload not only augments but is required for sunitinib-induced caspase 3/7 activation in human CMT (Figure 5B) suggests that the biomechanical loading intrinsic to the CMT model (and clinical sunitinib use) is an important regulator of sunitinib cardiac toxicity. The dependence of cardiotoxicity on in vitro afterload correlates well with clinical observations that development of LV dysfunction following sunitinib treatment is nearly always associated with hypertension. Our results suggest that human CMT may be the next step in improving our modeling of human sunitinib cardiotoxicity.

STUDY LIMITATIONS. One limitation of this study is using neonatal rat cells to model adult human cardiotoxicity. In the absence of an adult human cardiomyocyte cell line, NRVM have been used for years and are able to recapitulate many aspects of human cardiac biology. Nevertheless, we will ultimately be limited by interspecies differences. Though cardiac myocytes derived from Hu-iPS mitigate the species difference, these cells are also functionally immature. Another limitation is the inability to discern whether cells are becoming “sick” due to sunitinib and cannot generate as much force per cell or whether there are fewer live cells contributing to force generation. However, our results clearly demonstrate a decrease in the beating rates of live cells in CMT treated with sunitinib. This result suggests that sunitinib is making cells “sick” and less functional. Hence, it may be possible that sunitinib is affecting myocyte force generation independent of myocyte attrition due to apoptosis. Finally, our culturing of CMT on pillars with increased stiffness does not fully mimic the complex in vivo characteristics of ventricular-arterial coupling in a pulsatile flow environment and an onset of hypertension that is coincident with sunitinib exposure. Additional CMT model refinement to permit dynamic increases in afterload that better match in vivo conditions would further enhance the clinical relevance of this in vitro model system.

CONCLUSIONS

Overall, we are the first to describe using a 3D-engineered tissue platform to model human sunitinib cardiotoxicity. We recapitulated decreases in myocyte viability and function described in previous studies and demonstrated, for the first time, a loss of mitochondrial membrane potential with sunitinib treatment. We demonstrated that increased in vitro afterload augments the cardiotoxic effects of sunitinib in both rat and human CMT, supporting recent endorsement of aggressive blood pressure control during treatment with tyrosine kinase inhibitors (45).

ACKNOWLEDGMENTS The authors acknowledge the technical assistance of Dr. Rosa Álvarez, Dr. Wenli Yang of Penn Institute for Regenerative Medicine iPS core facility, and Charles (Hank) Pletcher from University of Pennsylvania Flow Cytometry core facility.

ADDRESS FOR CORRESPONDENCE: Dr. Kenneth B. Margulies, Perelman School of Medicine, University of Pennsylvania, Smilow Center for Translational Research, 3400 Civic Center Boulevard, 11-101, Philadelphia, Pennsylvania 19104. E-mail: Kenneth.margulies@uphs.upenn.edu.

PERSPECTIVES

COMPETENCY IN MEDICAL KNOWLEDGE: Many studies cite an association between developing hypertension and the eventual development of LV dysfunction during or after sunitinib treatment. The contribution of increased afterload to sunitinib's cardiotoxic effects has been understudied. We report that increased afterload augments cardiotoxicity of sunitinib. Our results suggest that afterload reduction may be important for preventing eventual LV dysfunction in patients receiving sunitinib.

TRANSLATIONAL OUTLOOK: As tyrosine kinase inhibitors such as sunitinib continue to be widely used in the treatment of cancer, better preclinical models for identifying the risks and mechanisms of cardiotoxicity will be very important. We have created an in vitro model of sunitinib cardiotoxicity that allows us to identify effects on cell viability and cardiac function while accounting for biomechanical inputs. These models may also serve as robust tools for disease modeling.

REFERENCES

1. Gschwind A, Fischer OM, Ullrich A. The discovery of receptor tyrosine kinases: targets for cancer therapy. *Nat Rev Cancer* 2004;4:361-70.
2. Force T, Krause DS, Van Etten RA. Molecular mechanisms of cardiotoxicity of tyrosine kinase inhibition. *Nat Rev Cancer* 2007;7:332-44.
3. Shah RR, Morganroth J, Shah DR. Cardiovascular safety of tyrosine kinase inhibitors: with a special focus on cardiac repolarisation (QT interval). *Drug Saf* 2013;36:295-316.
4. Shah RR, Morganroth J. Update on cardiovascular safety of tyrosine kinase inhibitors: with a special focus on QT interval, left ventricular dysfunction and overall risk/benefit. *Drug Saf* 2015;38:693-710.
5. Gurevich F, Perazella MA. Renal effects of anti-angiogenesis therapy: update for the internist. *Am J Med* 2009;122:322-8.
6. Faivre S, Demetri G, Sargent W, Raymond E. Molecular basis for sunitinib efficacy and future clinical development. *Nat Rev Drug Discov* 2007;6:734-45.
7. Demetri GD, Van Oosterom AT, Garrett CR, et al. Efficacy and safety of sunitinib in patients with advanced gastrointestinal stromal tumour after failure of imatinib: a randomised controlled trial. *Lancet* 2006;368:1329-38.
8. Motzer RJ, Hutson TE, Tomczak P, et al. Sunitinib versus interferon alfa in metastatic renal-cell carcinoma. *N Engl J Med* 2007;356:115-24.
9. Tellì ML, Witteles RM, Fisher GA, Srinivas S. Cardiotoxicity associated with the cancer therapeutic agent sunitinib malate. *Ann Oncol* 2008;19:1613-8.
10. Di Lorenzo G, Autorino R, Bruni G, et al. Cardiovascular toxicity following sunitinib therapy in metastatic renal cell carcinoma: a multicenter analysis. *Ann Oncol* 2009;20:1535-42.
11. Zamorano JL, Lancellotti P, Rodriguez Muñoz D, et al. 2016 ESC Position Paper on cancer treatments and cardiovascular toxicity developed under the auspices of the ESC Committee for Practice Guidelines: the Task Force for cancer treatments and cardiovascular toxicity of the European Society of Cardiology (ESC). *Eur Heart J* 2016;37:2768-801.
12. Fabian MA, Biggs WH, Treiber DK, et al. A small molecule-kinase interaction map for clinical kinase inhibitors. *Nat Biotechnol* 2005;23:329-36.
13. Laderoute KR, Calaoagan JM, Madrid PB, Klon AE, Ehrlich PJ. SU11248 (sunitinib) directly inhibits the activity of mammalian 5'-AMP-activated protein kinase (AMPK). *Cancer Biol Ther* 2010;10:1-8.
14. Kerkela R, Woulfe KC, Durand JB, et al. Sunitinib-induced cardiotoxicity is mediated by off-target inhibition of AMP-activated protein kinase. *Clin Transl Sci* 2009;2:15-25.
15. Izumiya Y, Shiojima I, Sato K, Sawyer DB, Colucci WS, Walsh K. Vascular endothelial growth factor blockade promotes the transition from compensatory cardiac hypertrophy to failure in response to pressure overload. *Hypertension* 2006;47:887-93.
16. Zentilin L, Puligadda U, Lionetti V, et al. Cardiomyocyte VEGFR-1 activation by VEGF-B induces compensatory hypertrophy and preserves cardiac function after myocardial infarction. *FASEB J* 2010;24:1467-78.
17. Chintalgattu V, Ai D, Langley RR, et al. Cardiomyocyte PDGFR-beta signaling is an essential component of the mouse cardiac response to load-induced stress. *J Clin Invest* 2010;120:472-84.
18. Hellstrom M, Kalen M, Lindahl P, Abramsson A, Betsholtz C. Role of PDGF-B and PDGFR-beta in recruitment of vascular smooth muscle cells and pericytes during embryonic blood vessel formation in the mouse. *Development* 1999;126:3047-55.
19. Di Siena S, Gimmelli R, Nori SL, et al. Activated c-Kit receptor in the heart promotes cardiac repair and regeneration after injury. *Cell Death Dis* 2016;7:e2317.
20. Fernandes-Silva MM, Shah AM, Hedge S, et al. Race-related differences in left ventricular structural and functional remodeling in response to increased afterload: the ARIC Study. *J Am Coll Cardiol HF* 2017;5:157-65.
21. Chen XJ, Sun XL, Zhang Q, et al. Uncontrolled blood pressure as an independent risk factor of early impaired left ventricular systolic function in treated hypertension. *Echocardiography* 2016;33:1488-94.
22. Ozkan A, Kapadia S, Tuzcu M, Marwick TH. Assessment of left ventricular function in aortic stenosis. *Nat Rev Cardiol* 2011;8:494-501.
23. Astashkina A, Mann B, Grainger DW. A critical evaluation of in vitro cell culture models for high-throughput drug screening and toxicity. *Pharmacol Ther* 2012;134:82-106.
24. Seok J, Warren HS, Cuenca AG, et al., for the Inflammation and Host Response to Injury. Large Scale Collaborative Research Program. Genomic responses in mouse models poorly mimic human inflammatory diseases. *Proc Natl Acad Sci U S A* 2013;110:3507-12.
25. Legant WR, Pathakb A, Yang MT, Deshpande VS, McMeeking RM, Chen CS. Microfabricated tissue gauges to measure and manipulate forces from 3D microtissues. *Proc Natl Acad Sci U S A* 2009;106:10097-102.
26. Boudou T, Legant WR, Mu A, et al. A microfabricated platform to measure and manipulate the mechanics of engineered cardiac microtissues. *Tissue Eng Part A* 2012;18:910-9.
27. Ghelli A, Porcelli AM, Zanna C, Rugolo M. 7-Ketocholesterol and staurosporine induce opposite changes in intracellular pH, associated with distinct types of cell death in ECV304 cells. *Arch Biochem Biophys* 2002;402:208-17.
28. Nieminen AL, Saylor AK, Tesfai SA, Herman B, Lemasters JJ. Contribution of the mitochondrial permeability transition to lethal injury after exposure of hepatocytes to t-butylhydroperoxide. *Biochem J* 1995;307:99-106.
29. He Y, Huang 1, Farischoen C, et al. Combined effects of atorvastatin and aspirin on growth and apoptosis in human prostate cancer cells. *Oncol Rep* 2017;37:953-60.
30. Nguyen PD, Hsiao ST, Sivakumaran P, Lim SY, Dilley RJ. Enrichment of neonatal rat cardiomyocytes in primary culture facilitates long-term maintenance of contractility in vitro. *Am J Physiol Cell Physiol* 2012;303:C1220-8.
31. Houser SR, Margulies KB, Murphy AM, et al. Animal models of heart failure: a scientific statement from the American Heart Association. *Circ Res* 2012;111:131-50.
32. Ma SP, Vunjak-Novakovic G. Tissue-engineering for the study of cardiac biomechanics. *J Biomech Eng* 2016;138:021010.
33. Hasinoff BB, Patel D, O'Hara KA. Mechanisms of myocyte cytotoxicity induced by the multiple receptor tyrosine kinase inhibitor sunitinib. *Mol Pharmacol* 2008;74:1722-8.
34. Doherty KR, Wappel RL, Talbert DR, et al. Multi-parameter in vitro toxicity testing of crizotinib, sunitinib, erlotinib, and nilotinib in human cardiomyocytes. *Toxicol Appl Pharmacol* 2013;272:245-55.
35. Chu TF, Rupnick MA, Kerkela R, et al. Cardiotoxicity associated with tyrosine kinase inhibitor sunitinib. *Lancet* 2007;370:2011-9.
36. Maayah ZH, Ansari MA, El Gendy MA, Al-Arif MN, Korashy HM. Development of cardiac hypertrophy by sunitinib in vivo and in vitro rat cardiomyocytes is influenced by the aryl hydrocarbon receptor signaling pathway. *Arch Toxicol* 2014;88:725-38.
37. Lin EC, Holzem KM, Anson BD. Properties of WT and mutant hERG K channels expressed in neonatal mouse cardiomyocytes. *Am J Physiol Heart Circ Physiol* 2010;298:H1842-9.
38. Gilchrist KH, Lewis GF, Gay EA, Sellgren KL, Greg S. High-throughput cardiac safety evaluation and multi-parameter arrhythmia profiling of cardiomyocytes using microelectrode arrays. *Toxicol Appl Pharmacol* 2015;288:249-57.
39. Rainer PP, Doleschal B, Kirk JA, et al. Sunitinib causes dose-dependent negative functional effects on myocardium and cardiomyocytes. *BJU Int* 2012;110:1455-62.
40. French KJ, Coatney RW, Renninger JP, et al. Differences in effects on myocardium and mitochondria by angiogenic inhibitors suggest separate mechanisms of cardiotoxicity. *Toxicol Pathol* 2010;38:692-702.

41. Lakhani SA, Masud A, Kuida K, et al. Caspases 3 and 7: key mediators of mitochondrial events of apoptosis. *Science* 2006;311:847-51.

42. Safulina D, Veksler V, Zharkovsky A, Kaasik A. Loss of mitochondrial membrane potential is associated with increase in mitochondrial volume: physiological role in neurones. *J Cell Physiol* 2006;206:347-53.

43. Chintalgattu V, Rees ML, Culver JC, et al. Coronary microvascular pericytes are the cellular

target of sunitinib malate-induced cardiotoxicity. *Sci Transl Med* 2013;5:187ra69.

44. Cohen JD, Babiarz JE, Abrams RM. Use of human stem cell derived cardiomyocytes to examine sunitinib mediated cardiotoxicity and electrophysiological alterations. *Toxicol Appl Pharmacol* 2011;257:74-83.

45. Armenian SH, Lacchetti C, Barac A, et al. Prevention and monitoring of cardiac dysfunction in survivors of adult cancers: American Society of

Clinical Oncology Clinical Practice Guideline. *J Clin Oncol* 2017;35:893-911.

KEY WORDS afterload, apoptosis, cardiotoxicity, sunitinib, tissue engineering, toxicology, tyrosine kinase inhibitors

APPENDIX For supplemental material, figures, and references, please see the online version of this paper.